J. Fluid Mech. (1994), *vol.* 262, *pp.* 111–139

Compositional convection in the solidification of binary alloys

By P. W. EMMS AND A. C. FOWLER
Mathematical Institute, Oxford University, 24–29 St. Giles', Oxford OX1 3LB, UK

(Received 18 August 1992 and in revised form 3 September 1993)

When a binary alloy is directionally solidified, a two-phase mushy dendritic zone is often formed. Interdendritic convection of the melt may occur, and is coupled with compositional convection of the residual melt. If fluid flow velocities are high enough, local melt-back of the dendrites may occur, leading to channel formation, and thus preferred flow paths. In order to predict the onset of convection, a coupled liquid/mush model is proposed, which includes most of the known physics. An elaborate scaling procedure leads to certain conclusions concerning the nature of convection, and points to a much simplified model, which can essentially be solved analytically. Predictions of the theory are compared quantitatively with experiments.

1. Introduction

The solidification of multi-component fluids is complicated by their typical phase diagrams, which shows that such mixtures do not have a single temperature at which a change of phase occurs. Rather, there is a *solidus* curve (relating temperature to composition) above which solid begins to melt, and a higher *liquidus* curve, below which liquid begins to freeze. A common phase diagram is portrayed in figure 1, which is appropriate for many binary allows, and the caption to the figure describes the features of the diagram in further detail. The thermodynamics of the situation is described by Flemings (1974), for example. One consequence of phase diagrams, such as that in figure 1, is that as an alloy solidifies, there is rejection of one or other of the components into the melt. For example, a solidifying interface freezing a mixture of A and B will typically solidify either A or B (unless the temperature is eutectic, see figure 1), so that the other component will be rejected. An example is the freezing of brine, wherein pure ice is formed, and excess salt is rejected into the liquid (this is why sea ice is fresh): here the (solid) components are ice and salt. It is evident that if there is a density difference between the two components, then the freezing will act as a buoyancy source or sink, depending on the direction of freezing. Thus compositional convection is likely to occur or, since temperature is also involved, some form of double-diffusive convection (Huppert 1990).

A further consequence of this rejection is that a compositional boundary layer builds up ahead of an advancing interface. Since it is typically the case that the Lewis number ($Le = \kappa_l/D$ = thermal diffusivity/solute diffusivity) is large, the temperature hardly changes through this boundary layer, and as a result, since the liquidus temperature depends on concentration, the compositional boundary layer is often supercooled. Although some degree of supercooling is necessary for crystal growth, too much renders an advancing planar interface unstable, and a branching dendritic *mushy zone* results, which separates solid from liquid (Flemings 1974). This mushy zone consists of

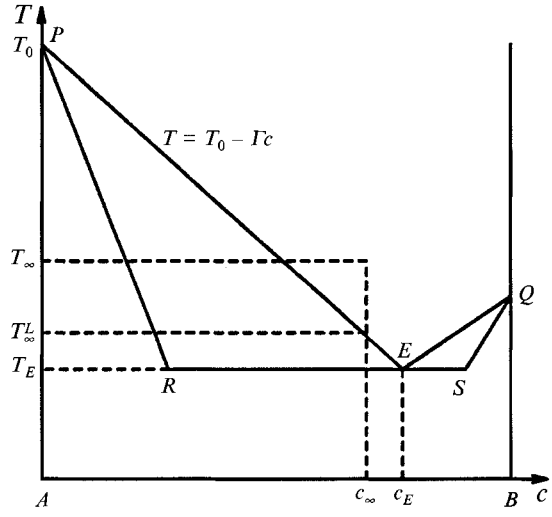

FIGURE 1. Schematic phase diagram for a binary alloy with components A and B. The liquidus curve is represented by PEQ, the eutectic point is E, and c_∞, T_∞ are the initial composition and temperature of the alloy. The solidus curves are PR and QS.

a porous maze of dendritic solid and residual interstitial liquid, and if the rejected liquid is lighter than the bulk liquid, compositional convection can take place both in the liquid and in the mush.

The particular phenomenon we are concerned with here occurs when convection in the mush becomes too vigorous. In particular, if the liquid velocity exceeds the solidification rate, local re-melting of dendrites will occur, leading to increased convective flow (due to increased permeability) and the resultant formation of flow channels of liquid only. These channels then dictate the convective style of flow. Evidence of such channel formation can be observed in metal alloy castings, since in the final solidified form the channels solidify later and with a different composition than the surrounding mush. These 'freckles' cause problems in the metallurgical industries, and formed the initial motivation for the study of their formation (Flemings & Nereo 1967; McDonald & Hunt 1969, 1970; Mehrabian, Keane & Flemings 1970*a b*; Copley *et al.* 1970; Szekely & Jassal 1978). They are seen in low-entropy materials, whose growth is non-faceted and thus properly dendritic (Woodruff 1973), such as metal alloys and a few non-metals, most notably ammonium chloride, which is a convenient material for experiment.

The purpose of this paper is to establish a realistic scenario for the onset and development of convection and flow channels in dendritically solidifying binary alloys. The emphasis is on a quantitative understanding of the processes involved, with a view to specific prediction as to when they will occur. There have been a number of other models used to predict the flow patterns in situations of this type. Whereas these can be successful (Kou, Poirier & Flemings 1978; Szekely & Jassal 1978; Ridder, Kou & Mehrabian 1981; Fujii, Proctor & Flemings 1979; Maples & Poirier 1984; Thompson & Szekely 1988), they tend not to include all the physics in a rational way. Thus our intention is rather different: to avoid any arbitrary or unwarranted assumptions. In particular, convection in both liquid and mush will be included in the model, and its effects will be studied analytically rather than computationally. The crucial usefulness of this approach is that it may, in principle, help us to extrapolate the analysis to much larger-scale solidifying alloys – the Earth's core and crystallizing magma chambers are

two possible examples (Jacobs 1953; Loper & Roberts 1978, 1980, 1981), although it should be emphasized that these systems (particularly the Earth's core) may be far from eutectic, contrary to what is assumed herein.

On the more formal and deductive side of an approach to this problem, there have been several recent efforts, both in model formulation and analysis. Principal amongst these is the paper by Hills, Loper & Roberts (1983), which provides a complete model for a mushy zone. Their motivation is also the solidification of the Earth's core, and a more practical reduction of this model is given by Roberts & Loper (1983), seeking to understand the experiments by Copley *et al.* (1970) on NH_4Cl. Worster (1986), following earlier work by Huppert & Worster (1985), took a simpler approach, omitting considerations of convective flow but seeking to find realistic (similarity) solutions to laboratory experimental conditions. His results for growth rate showed good agreement with experiments on ice growing from aqueous sodium nitrate. Fowler (1985) extended Worster's model to include convection (his model is also included in that of Hills *et al.*), and studied the onset of convection at prescribed constant solidification rate. He was able to partly analyse the system, but only by parameterizing convection in the liquid in a kinematic (probably unrealistic) way. Worster (1992) has also extended his (1986) model to include the effects of fluid flow. He then performed a linear stability analysis on the coupled liquid/mush equations. Two modes of instability were found: a boundary-layer mode corresponding to finger-like convection, and a mushy-layer mode in which convection is initiated on a much larger lengthscale. When the mushy layer is sufficiently small, the former mode will occur first (as is usually observed), and so we will restrict our attention to this case.

Volume-averaged equations for alloy solidification have been proposed by Beckermann & Viskanta (1988), Ganesan & Poirier (1990), and Ni & Beckermann (1991). The advantage of averaging is that one can see how the macroscopic and microscopic variables are related. The disadvantage is that a description of appropriate constitutive relations is difficult. Beckermann & Viskanta (1988) described a volume-averaged model using the methods developed for studying multiphase regions. The equations were solved numerically for a vertical rectangular enclosure containing ammonium chloride solution being solidified from the side. However, their results show considerable disagreement with experimental data. An explicit derivation of the averaging technique has been presented by Ganesan & Poirier (1990). They derived mass and momentum equations for the mush, and considered Darcy's law as an approximation to the momentum equation. Ni & Beckermann (1991) have derived in detail a two-phase model for transport phenomena during solidification. The model includes enthalpy, concentration and velocity variables for both the solid and liquid phases, and non-equilibrium effects are also incorporated.

Recently Bennon & Incropera (1987*a*) have formulated a continuum model based upon the principles of classical mixture theory. Their equations have the advantage of being valid in each phase (solid, mush, liquid). This makes them amenable to a numerical solution because there is no need to track, and pose boundary conditions on, the moving phase interfaces. Using the model, Neilson & Incropera (1991) were able to simulate numerically the induced fluid flow and channel development within the mush of an $NH_4Cl.H_2O$ model alloy. Their results appear to agree qualitatively with the experimental observations of Sample & Hellawell (1982, 1984).

The solidification of a metal alloy cooled from the sides has been studied by Amberg (1991). The time-dependent equations were solved numerically up to the point of complete solidification. The macrosegregation (solute redistribution) was then calculated at various times throughout the solidification process. However, channel

segregation within the final solidified metal ingot was not discussed. Amberg & Homsy (1993) have recently analysed the nonlinear stability of Worster's (1991) model, with a view to studying chimney formation in more detail. It was found that both subcritical and supercritical instabilities could occur depending on the values of the parameters.

In this paper we will extend Worster's (1986) analysis to include a more realistic account of convection in the liquid as well as that in the mush. We are thus led to a scaling analysis which seems in accord with many of the observations by Sample & Hellawell (1982, 1984), Sarazin & Hellawell (1988) and Tait & Jaupart (1992). In particular, our analysis is consistent with an initial phase when convection is absent, a second phase when finger-like convection can be seen in the liquid, before channels form, which heralds a third phase. The analysis of this third phase is beyond the present scope, but has been studied by Roberts & Loper (1983), and by Worster (1991).

2. Mathematical model and non-dimensionalization

Model equations describing convection in the porous dendritic mush have been given by Fowler (1985), Worster (1986), and Hills *et al.* (1983). We take them in the form

$$\rho_t + \nabla \cdot [\rho \boldsymbol{u}] = 0, \tag{2.1a}$$

$$-L\frac{\partial}{\partial t}[\rho(1-\chi)] + \rho[\chi c_l + (1-\chi)c_s]\frac{\partial T}{\partial t} + \rho c_l \boldsymbol{u} \cdot \nabla T = \nabla \cdot [k \nabla T], \tag{2.1b}$$

$$\rho \frac{\mathrm{d}}{\mathrm{d}t}(\chi c) + \nabla \cdot [\rho(1-\chi)c\boldsymbol{u}] = \nabla \cdot [\rho \chi D \nabla c], \tag{2.1c}$$

$$\boldsymbol{u} = -(\Pi/\mu)[\nabla p + \rho_l g \boldsymbol{k}], \tag{2.1d}$$

$$\rho = \frac{\rho_l}{1 - r(1-\chi)}, \tag{2.1e}$$

$$\rho_l = \rho_l^0[1 - \alpha_l(T - T_L^\infty) - \beta_l(c - c_\infty)], \tag{2.1f}$$

$$k = \frac{\rho \chi k_l}{\rho_l} + \frac{\rho(1-\chi)k_s}{\rho_s}, \tag{2.1g}$$

where ρ is density, c is liquid composition, χ is liquid mass fraction, T is temperature, and $\boldsymbol{u}$ is the liquid flux ($= \chi \times$ liquid velocity). In addition, we assume that in the mush, thermodynamic equilibrium prevails, so that the average temperature is at the liquidus, which we suppose to be given by

$$T = T_0 - \Gamma c, \tag{2.2}$$

and that the partition coefficient is zero, so that the solid concentration is zero.

The material derivative in (2.1) is defined by $\mathrm{d}/\mathrm{d}t = \partial/\partial t + \boldsymbol{u} \cdot \nabla$. The constants in (2.1) are L, the latent heat; c_s and c_l, the specific heats of solid and liquid; k_s and k_l, the thermal conductivities; D, the solute diffusivity in the liquid (we assume it to be zero in the solid); Π, the permeability; μ, the dynamic viscosity; ρ_l, the liquid density; g is gravity, $\boldsymbol{k}$ a unit vector in the vertical z-direction, ρ_s is the solid density, and r is defined by

$$r = (\rho_s - \rho_l)/\rho_s. \tag{2.3}$$

The coefficients α_l and β_l are coefficients of thermal and compositional expansion; T_L^∞ and c_∞ are defined below. These equations represent conservation of mass, energy, solute, and liquid momentum (Darcy's law). We suppose the solid is immobile.

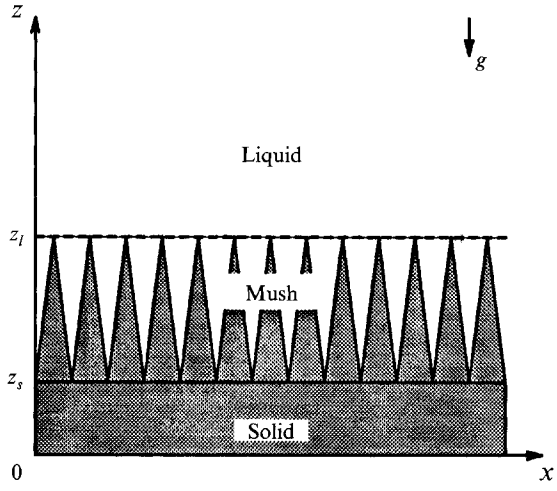

FIGURE 2. Schematic of a vertically solidifying alloy.

Equations in the liquid and solid regions ($\chi = 1$ and $\chi = 0$) are more straightforward. In the liquid, we prescribe (anticipating the Boussinesq approximation)

$$\nabla \cdot \boldsymbol{u} = 0, \tag{2.4a}$$

$$\frac{\mathrm{d}T}{\mathrm{d}t} = \kappa_l \nabla^2 T, \quad \frac{\mathrm{d}c}{\mathrm{d}t} = D\nabla^2 c, \tag{2.4b, c}$$

$$\rho \frac{\mathrm{d}\boldsymbol{u}}{\mathrm{d}t} = -\nabla p + \mu_l \nabla^2 \boldsymbol{u} - \rho_l g \boldsymbol{k}, \tag{2.4d}$$

and in the solid

$$T_t = \kappa_s \nabla^2 T, \tag{2.5}$$

where κ_s is the solid thermal diffusivity. Since we will be interested in the upwards growth of a solidifying alloy, we shall assume the geometry sketched in figure 2.

There are two principal cases of interest. If the basal temperature is below eutectic (see figure 1), then eutectic solid ($\chi = 0$) grows from the base, whereas if the basal temperature is above the eutectic, solid is of one component only, and complete freezing cannot occur. This is obviously of less interest metallurgically, although it is more easily done in laboratory experiments (on aqueous solutions, for example).

We apply the following boundary conditions:

(i) On the liquid–mush interface, $z = z_l$:

$$V_n[\rho]^+_- = [\rho u_n]^+_-, \quad V_n[\rho\chi c]^+_- = \left[\rho c u_n - \rho\chi D \frac{\partial c}{\partial n}\right]^+_-, \tag{2.6a, b}$$

$$[T]^+_- = 0, \quad V_n[\rho\chi L]^+_- = \left[\rho L u_n - k\frac{\partial T}{\partial n}\right]^+_-, \tag{2.6c, d}$$

$$[c]^+_- = 0, \quad [p]^+_- = 0, \quad \chi = 1. \tag{2.6e–g}$$

These represent respectively, conservation of mass, conservation of solute, thermodynamic equilibrium, conservation of energy, solutal equilibrium, force balance, and lastly a condition representing continuity of liquid fraction. The merits of some of these conditions are discussed by Fowler (1985), Worster (1986), and Hills *et al.* (1983). '$[\,]^+_-$' represents a jump from z_l^+ to z_l^-, and a subscript n means the normal component. V is the velocity of z_l.

(ii) On the solid–mush interface, $z = z_s$:

$$V_n[\rho]_-^+ = [\rho u_n]_-^+, \quad c = c_E \quad \text{(eutectic)} \tag{2.7a, b}$$

or

$$V_n[\rho\chi c]_-^+ = \left[\rho c u_n - \rho\chi D\frac{\partial c}{\partial n}\right]_-^+, \tag{2.7c}$$

$$[T]_-^+ = 0, \quad V_n[\rho L\chi]_-^+ = \left[\rho L u_n - k\frac{\partial T}{\partial n}\right]_-^+. \tag{2.7d, e}$$

(iii) At the container base, $z = 0$:

$$T = T_b \quad \text{(for example)}. \tag{2.8}$$

The alternatives in (2.7*b*, *c*) arise depending on whether growth is eutectic or not. Notice that $V_n = \dot{z}_s$ in (2.7), but $V_n = \dot{z}_l$ in (2.6). We wish to solve (2.1), (2.2), (2.4), (2.5) with boundary conditions (2.6), (2.7), (2.8). We have not explicitly posed boundary conditions at the top surface of the liquid; we shall generally suppose 'far-field' conditions such as

$$T \to T_\infty, \quad c \to c_\infty \quad \text{as} \quad z \to \infty. \tag{2.9}$$

Conditions on p and $\boldsymbol{u}$ will not be needed explicitly.

2.1. *Non-dimensionalization*

We begin by non-dimensionalizing the problem. If d is a representative lengthscale for the system (e.g. the depth of the initial fluid), then a thermal velocity scale is $V = \kappa_l/d$, and we use this in scaling $\boldsymbol{x}$ and $\boldsymbol{u}$. This is apparently inconsistent with far-field boundary conditions such as (2.9), but in fact we are more concerned with the depth of mush at the onset of convection, and this is typically a good deal smaller than d. Moreover, we shall find later that the relevant lengthscale in the liquid region is much less than d, which justifies the use of (2.9) *a posteriori*.

There are two natural temperature scales in the system. If T_L^∞ denotes the liquidus temperature in the far field of the liquid, that is $T_L^\infty = T_0 - \Gamma c_\infty$, then $T_\infty - T_L^\infty$ is the liquid superheat, while $T_L^\infty - T_E$ is the mush temperature range, where T_E is the eutectic temperature, $T_E = T_0 - \Gamma c_E$, and c_E is the eutectic composition.

In order to make use of the possibility that the initial composition is close to the eutectic, we scale the composition with the difference $c_E - c_\infty$, taken as positive. Thus we define

$$\left.\begin{gathered} \boldsymbol{x} = \mathrm{d}\boldsymbol{x}^*, \quad \boldsymbol{u} = (\kappa_l/d)\,\boldsymbol{u}^*, \quad t = (d^2/\kappa_l)\,t^*, \\ \rho = \rho_l^0\rho^*, \quad T = T_L^\infty + (T_L^\infty - T_E)\,T^*, \quad c = c_\infty + (c_E - c_\infty)\,c^*, \\ p = p_\infty - \rho_l^0 gz + (\mu\kappa_l/\Pi_0)\,p^*, \quad \Pi = \Pi_0\Pi^*, \end{gathered}\right\} \tag{2.10}$$

where Π_0 is a permeability scale, p_∞ is the ambient pressure, and μ is the liquid viscosity. Substituting these into the governing equations and boundary conditions, we obtain the following, where we have dropped the asterisks.

(*a*) In the mush:

$$T = -c, \quad \boldsymbol{u} = -\Pi(\chi)[\nabla p - Rc\boldsymbol{k}], \tag{2.11a, b}$$

$$\rho = [1 - r(1-\chi)]^{-1}, \quad \rho_t + \nabla\cdot[\rho\boldsymbol{u}] = 0, \tag{2.11c, d}$$

$$\rho\frac{\mathrm{d}}{\mathrm{d}t}[\chi(1+\beta c)] + \nabla\cdot[\rho(1-\chi)(1+\beta c)\,\boldsymbol{u}] = \frac{\beta}{Le}\nabla\cdot[\rho\chi\nabla c], \tag{2.11e}$$

$$-\frac{S}{\beta}\frac{\partial}{\partial t}[\rho(1-\chi)] + \rho\bar{c}\frac{\partial T}{\partial t} + \rho\boldsymbol{u}\cdot\nabla T = \nabla\cdot[\bar{k}\nabla T], \tag{2.11f}$$

where
$$\left.\begin{aligned} \beta = \frac{c_E - c_\infty}{c_\infty}, \quad Le = \frac{\kappa_l}{D}, \quad S = \frac{L}{c_l \Gamma c_\infty} = \frac{L}{c_l (T_0 - T_L^\infty)}, \\ \bar{c} = \chi + \frac{(1-\chi)\, c_s}{c_l}, \quad \bar{k} = \rho\chi + \rho(1-r)(1-\chi)\frac{k_s}{k_l}, \\ R = \frac{\Delta\rho g d \Pi_0}{\mu\kappa_l}, \end{aligned}\right\} \tag{2.12}$$

and
$$\Delta\rho = \rho_l^0[\beta_l(c_E - c_\infty) - \alpha_l(T_L^\infty - T_E)] \tag{2.13}$$

is the density difference between the far-field liquidus density and that of the eutectic liquid. The parameters are Le, the Lewis number, R, a Rayleigh number, and S, related to the Stefan number.

(*b*) In the liquid:
$$\nabla \cdot \boldsymbol{u} = 0, \tag{2.14a}$$
$$\frac{\mathrm{d}T}{\mathrm{d}t} = \nabla^2 T, \quad \frac{\mathrm{d}c}{\mathrm{d}t} = \frac{1}{Le}\nabla^2 c, \tag{2.14b, c}$$
$$\left[\frac{\gamma}{\sigma(1-r)}\right]\frac{\mathrm{d}\boldsymbol{u}}{\mathrm{d}t} = -\nabla p + \gamma\nabla^2\boldsymbol{u} + (R_\alpha T + R_\beta c)\,\boldsymbol{k}, \tag{2.14d}$$

where the Prandtl number is
$$\sigma = \mu_l/\rho_l\kappa_l, \tag{2.15}$$

thermal and compositional Rayleigh numbers are
$$R_\alpha = \frac{\rho_l^0 \alpha_l (T_L^\infty - T_E) g \Pi_0 d}{\mu\kappa_l}, \quad R_\beta = \frac{\rho_l^0 \beta_l (c_E - c_\infty) g \Pi_0 d}{\mu\kappa_l}, \tag{2.16a, b}$$

and the parameter γ, given by
$$\gamma = \Pi_0^2/d^2, \tag{2.17}$$

is a measure of the dendritic spacing, since if l is the dendrite spacing scale, then since $\Pi_0 \sim l^2$,
$$\gamma \leqslant l^2/d^2. \tag{2.18}$$

(Note that $\gamma^{-1} = \mathscr{H}$ as defined by Worster 1992.)

(*c*) In the solid:
$$T_t = \frac{\kappa_s}{\kappa_l}\nabla^2 T. \tag{2.19}$$

The boundary conditions we apply are as follows:

(i) In the liquid, as $z \to \infty$:
$$T \to \Delta_\infty, \quad c \to 0, \tag{2.20}$$

where
$$\Delta_\infty = \frac{T_\infty - T_L^\infty}{T_L^\infty - T_E}. \tag{2.21}$$

(ii) On the liquid–mush interface, $z = z_l$:
$$V_n[\rho]_-^+ = [\rho u_n]_-^+, \quad V_n[\rho\chi(1+\beta c)]_-^+ = \left[\rho(1+\beta c)\, u_n - \frac{\beta}{Le}\rho\chi\frac{\partial c}{\partial n}\right]_-^+, \tag{2.22a, b}$$
$$[T]_-^+ = 0, \quad V_n[S\rho\chi]_-^+ = \left[S\rho u_n - \beta\bar{k}\frac{\partial T}{\partial n}\right]_-^+, \tag{2.22c, d}$$
$$[c]_-^+ = 0, \quad [p]_-^+ = 0, \quad \chi = 1. \tag{2.22e–g}$$

(iii) On the solid–mush interface, $z = z_s$:

$$V_n[\rho]_-^+ = [\rho u_n]_-^+, \quad c = 1, \quad \text{(eutectic)} \tag{2.23a, b}$$

or

$$V_n[\rho\chi(1+\beta c)]_-^+ = \left[\rho(1+\beta c)\,u_n - \frac{\beta}{Le}\rho\chi\frac{\partial c}{\partial n}\right]_-^+, \tag{2.23c}$$

$$[T]_-^+ = 0, \quad V_n[S\rho\chi]_-^+ = \left[S\rho u_n - \beta\bar{k}\frac{\partial T}{\partial n}\right]_-^+; \tag{2.23d, e}$$

at the container base,

$$T = \Delta_b, \tag{2.24}$$

where

$$\Delta_b = \frac{T_b - T_L^\infty}{T_L^\infty - T_E}. \tag{2.25}$$

We now wish to solve (2.11), (2.14) and (2.19) subject to (2.20), (2.22), (2.23) and (2.24).

3. Scaling the model

We begin by estimating the orders of magnitude of the various dimensionless constants of the model, which are: $\beta, S, Le, R, \sigma, R_\alpha, R_\beta, \gamma, r, \Delta_\infty, \Delta_b$. Obviously these will vary depending on the application, but we shall choose for illustration those appropriate to laboratory ammonium chloride experiments: see Chen & Chen (1991), Tait & Jaupart (1992), Sarazin & Hellawell (1988), Bennon & Incropera (1987*b*), or Szekely & Jassel (1978), denoted CC, TJ, SH, BI and SJ respectively. We choose

$$\left.\begin{aligned}
&L \sim 3.14\times10^2\ \text{kJ kg}^{-1}, \quad c_p \sim 3.25\ \text{kJ kg}^{-1}\text{K}^{-1} \quad \text{(BI)},\\
&\Gamma \sim 490\ \text{K} \quad \text{(TJ)},\\
&\kappa \sim 1.47\times10^{-3}\ \text{cm}^2\,\text{s}^{-1}, \quad D \sim 1.3\times10^{-5}\ \text{cm}^2\,\text{s}^{-1} \quad \text{(SH)},\\
&\rho_l^0 \sim 1.08\times10^3\ \text{kg m}^{-3} \quad \text{(SJ)},\\
&\rho_s \sim 1.52\times10^3\ \text{kg m}^{-3} \quad \text{(CC)},\\
&\beta_l \sim 0.3 \quad \text{(BI)},\\
&\alpha_l \sim 2\times10^{-4}\ \text{K}^{-1} \quad \text{(SJ)},\\
&g \sim 10^3\ \text{cm s}^{-2},\\
&l \sim 10^{-1}\ \text{cm} \quad \text{(SJ)},\\
&\mu_l \sim 1.03\times10^{-2}\ \text{gm cm}^{-1}\,\text{s}^{-1} \quad \text{(SH)},\\
&d \sim 10\ \text{cm}.
\end{aligned}\right\} \tag{3.1}$$

We take $c_E = 0.8$, $T_E = -15\ ^\circ\text{C}$, and choose representative values $c_\infty = 0.75$, $T_b = -50\ ^\circ\text{C}$, $T_\infty = 50\ ^\circ\text{C}$; we also take $\Pi_0 = l^2/100 \sim 10^{-4}\ \text{cm}^2$; then $V \sim 1.5\times10^{-2}\ \text{cm s}^{-1}$, $T_L^\infty = 9.5\ ^\circ\text{C}$, and

$$\left.\begin{aligned}
&\beta \sim 0.067, \quad S \sim 0.25, \quad R_\alpha \sim 0.5\times10^3, \quad R_\beta \sim 1.5\times10^3,\\
&R = R_\beta - R_\alpha \sim 10^3, \quad \sigma \sim 10, \quad \gamma \sim 10^{-6}, \quad r \sim 0.3, \quad \Delta_b = -2.4, \quad \Delta_\infty = 1.6.
\end{aligned}\right\} \tag{3.2}$$

3.1. *Initial approximations*

The first (and least accurate) approximation we make is an extended Boussinesq approximation:

$$r = 0; \tag{3.3}$$

thus we neglect solidification shrinkage, in the time-honoured tradition that the important density changes are those associated with buoyancy in the liquid. For some

alloys (e.g. Pb–Sn) (3.3) is quite accurate ($r \sim 0.03$). Actually, as we are soon to take $1-\chi$ as small, (3.3) will even be accurate for NH_4Cl (in the sense that $\rho \approx$ constant, if the composition is nearly eutectic). We further assume that Le is large, and put

$$1/Le = 0, \tag{3.4}$$

in the mush (but not in the liquid); this has been shown to be a regular approximation by Fowler (1985). We assume the initial liquid composition is close to eutectic; specifically, we taken $\beta \ll 1$, and rescale χ by writing

$$\chi = 1-\beta\phi. \tag{3.5}$$

Neglecting terms of order β, r and Le^{-1}, the equations in the mush can now be simplified, yielding

$$\nabla \cdot \boldsymbol{u} = 0, \quad \frac{\partial \phi}{\partial t} = \frac{\mathrm{d}c}{\mathrm{d}t}, \tag{3.6a, b}$$

$$(1+S)\frac{\mathrm{d}c}{\mathrm{d}t} = \nabla^2 c, \quad \boldsymbol{u} = -\nabla p + Rc\boldsymbol{k}, \tag{3.6c, d}$$

where we take $\Pi = 1$ (usual forms for Π have $\Pi \to 1$ as $\chi \to 1$, e.g. $\Pi \propto (1-\chi)^m$, $m = 2$ or 3).

The corresponding reduced boundary conditions are as follows:

On $z = z_l$:

$$\phi = 0, \quad [u_n]^+_- = 0, \quad [p]^+_- = 0, \quad [c]^+_- = 0, \tag{3.7a–d}$$

$$\left[\frac{\partial T}{\partial n}\right]^+_- = 0, \quad [T]^+_- = 0, \quad \left[\frac{\partial c}{\partial n}\right]^+_- = 0. \tag{3.7e–g}$$

The last condition follows from (2.22*b*) with $Le < \infty$, since all the other terms are continuous across z_l. It corresponds to a condition of marginal supercooling of the interface (cf. Worster 1986).

On $z = z_s$:

$$u_n^+ = 0, \quad [T]^+_- = 0, \quad SV_n = \beta\left[-\bar{k}\frac{\partial T}{\partial n}\right]^+_-, \tag{3.8a–c}$$

$$c = 1 \quad \text{or} \quad V_n \approx 0; \tag{3.8d, e}$$

the alternative in (3.8*e*) requires interpretation: it simply implies that when $Le \gg 1$ there is essentially no completely solid region; in that case $z_s = 0$, and we have $T = \Delta_b$ there also.

At this point we must make an intelligent guess about how solutions to this coupled system will behave. This is based partly on observation (Sample & Hellawell 1984) and partly on previous analysis of the model (Fowler 1985). The mush equations are essentially those describing convection in a porous medium, whereas those in the liquid describe double-diffusive finger-type convection (Turner 1973). (We are here assuming that $R_\alpha, R_\beta > 0$, i.e. release of buoyant fluid when cooled from below.) One cannot occur without the other since convection in one necessitates a horizontal compositional gradient at z_l, which would drive convection in the other. However, because of the negligible resistance of the liquid (i.e. because $\gamma \ll 1$), the liquid convection will be vigorous even if the convection in the dendrites is marginal. Consequently, either turbulent convection, or at least 'high Rayleigh number' convection (with boundary layers) will ensue in the liquid. If turbulent, we would parameterize the fluxes (Turner 1973); some of the experimental observations of Sample & Hellawell (1984) suggest

that convection in the liquid can be basically laminar, if time-dependent: vertical plumes of buoyant liquid wander about the liquid/mush interface. Insofar as the equations in the mush may be derived using averages in both time and space (Drew & Wood 1985), we can expect that such wandering plumes are consistent with a 'steady' flux from the mush, and that the spatial variation in this flux will control just how the plumes wander.

3.2. *Compositional convection*

We now wish to characterize the boundary-layer nature of the convection in the liquid. Suppose that there is a compositional boundary layer of thickness $\delta\epsilon$. Since the flux from the mush is $\partial c/\partial n \sim O(1)$, the change in c across the layer is $c \sim O(\delta\epsilon)$. Let us suppose appropriate scales for $t, \boldsymbol{x}, u$ in the liquid are $[t], \epsilon, [u]$. By rescaling with these values, and c with $\delta\epsilon$, we obtain the equations (putting $r = 0$)

$$\frac{\mathrm{d}c}{\mathrm{d}t} = \frac{1}{Le\epsilon[u]}\nabla^2 c, \tag{3.9}$$

$$\frac{[u]\epsilon}{\sigma}\frac{\mathrm{d}\boldsymbol{u}}{\mathrm{d}t} = -\frac{\epsilon}{\gamma[u]}\nabla p + \nabla^2\boldsymbol{u} + \frac{R_\beta \delta\epsilon^3}{\gamma[u]}c\boldsymbol{k}, \tag{3.10}$$

where we have chosen $[t] = \epsilon/[u]$, and omitted the thermal buoyancy term. Now the boundary-layer analysis of Roberts (1977, 1979), cf. Proctor (1981), implies that we should choose

$$\delta^3 = \frac{1}{Le\epsilon[u]}, \quad \frac{R_\beta \delta\epsilon^3}{\gamma[u]} = \frac{1}{\delta^2}. \tag{3.11a, b}$$

The lateral lengthscale ϵ is chosen consistently with the dynamics of finger-type convection. The exact solution of Stern (1975, chap. XI) and the more recent boundary-layer analysis of Howard & Veronis (1987) are both consistent with the idea that the width of the convective fingers is controlled by thermal diffusion, in the following sense. The flow in the fingers is controlled by compositional buoyancy. Since $Le \ll 1$, compositional variations occur over narrower regions than thermal variations. We can expect the temperature to vary across a finger (otherwise it is hardly a double-diffusive phenomenon) and we suppose that the finger width is such that the temperature variation is spread across each finger. A consequence of this is that thermal advection balances thermal conduction in the fingers, and the compositional variations occur across thinner boundary layers at the edges of fingers. Since T satisfies

$$\frac{\mathrm{d}T}{\mathrm{d}t} = \frac{1}{\epsilon[u]}\nabla^2 T, \tag{3.12}$$

we therefore choose

$$[u] = 1/\epsilon. \tag{3.13}$$

It then follows that

$$\delta = Le^{-\frac{1}{3}}, \quad [u] = (R_\beta/Le\gamma)^{\frac{1}{3}}. \tag{3.14a, b}$$

If we take $Le = 10^2$, $\gamma = 10^{-6}$, $R_\beta = 10^3$, then

$$\delta \sim 0.2, \quad [u] \sim 56, \quad \epsilon \sim 0.017, \quad p \sim \gamma[u]^2 \sim 0.003. \tag{3.15}$$

These estimates suggest fluid velocities in the fingers $\sim [u]V \sim 0.8\ \mathrm{cm\ s^{-1}}$, and finger widths $\sim \epsilon d \sim 0.17$ cm, and seem broadly consistent with observations. With $p \sim \gamma[u]^2 \ll 1, c \sim \epsilon\delta \ll 1, [u] \gg 1$, then we have approximate boundary conditions for the mush:

$$p = 0, \quad c = 0, \quad \phi = 0 \quad \text{at} \quad z_l, \tag{3.16a–c}$$

while at $z = z_s$,

$$u_n = 0, \quad c = 1. \tag{3.17a, b}$$

The mush equations (3.6) with the boundary conditions in (3.16) and (3.17) are precisely the equations for convection in a porous medium, and the equation for ϕ uncouples.

The lower boundary z_s is determined by the Stefan condition for its normal velocity:

$$V_n = \frac{\beta}{S}\left[-\bar{k}\frac{\partial T}{\partial n}\right]_-^+, \tag{3.18}$$

or $V_n \approx 0$ if $T_b > T_E$. The final condition to determine z_l follows from the flux conditions in (3.7), which in rescaled form, for each layer, can be written (with $\boldsymbol{n} = \epsilon \boldsymbol{N}$)

$$\frac{1}{\epsilon}\frac{\partial T}{\partial N_+} = -\delta\frac{\partial c}{\partial N_+} = -\frac{\partial c}{\partial n_-}. \tag{3.19a–c}$$

Equation (3.19*b*) gives the compositional flux condition for the liquid, and (3.19*a*) gives the extra condition, since we also have

$$T = 0, \quad \boldsymbol{u} = \boldsymbol{0} \quad \text{at} \quad z_l^+. \tag{3.20}$$

4. Asymptotic solution

4.1. *Boundary-layer description of convection in the liquid*

In the liquid, we have (with the smaller lengthscale $\sim \epsilon$, timescale ϵ^2, velocity scale $1/\epsilon$, pressure scale γ/ϵ^2, and rescaling c with $\delta\epsilon$)

$$\nabla \cdot \boldsymbol{u} = 0, \quad c_{t'} + \boldsymbol{u} \cdot \nabla c = \delta^3 \nabla^2 c, \tag{4.1a, b}$$

$$\frac{1}{\sigma}\frac{\mathrm{d}\boldsymbol{u}}{\mathrm{d}t'} = -\nabla p + \nabla^2 \boldsymbol{u} + \frac{c}{\delta^2}\boldsymbol{k}, \quad T_{t'} + \boldsymbol{u} \cdot \nabla T = \nabla^2 T, \tag{4.1c, d}$$

where $t = \epsilon^2 t'$, together with

$$-\delta\frac{\partial c}{\partial N}\bigg|_{z_l^+} = G = -\frac{\partial c}{\partial n}\bigg|_{z_l^-}, \quad T = 0, \quad \boldsymbol{u} = \boldsymbol{0}, \tag{4.2a–e}$$

on z_l, and

$$T \to \Delta_\infty, \quad c \to 0 \quad \text{as} \quad z \to \infty. \tag{4.3a, b}$$

The far-field condition on $\boldsymbol{u}$ might be taken as $\boldsymbol{u} \to \boldsymbol{0}$, on the basis that the finger cells merge. Lower down, a more appropriate condition for the boundary-layer solution may be that $\boldsymbol{u} \to (0, w(X))$ where X is the horizontal coordinate. The free boundary is determined by the final condition,

$$\frac{\partial T}{\partial N} = \epsilon G \quad \text{at} \quad z_l. \tag{4.4}$$

The boundary-layer solution is modified from that of Roberts (1979), and is detailed in Appendix A. The temperature field uncouples from the compositional field providing thermal buoyancy is negligible (an unrealistic assumption), and the solution thus determines $\boldsymbol{u}$ as an $O(1)$ function. Given this $\boldsymbol{u}$, we thus have to solve

$$T_{t'} + \boldsymbol{u} \cdot \nabla T = \nabla^2 T, \tag{4.5}$$

$$T \to \Delta_\infty \quad \text{as} \quad z \to \infty, \tag{4.6a}$$

$$T = 0, \quad \frac{\partial T}{\partial N} = \epsilon G \quad \text{on} \quad z_l, \tag{4.6b, c}$$

where $G = O(1)$.

The solution is as follows, and is detailed in Appendix B. Essentially the thermal profile in the liquid evolves on the slow conductive timescale $t = \epsilon^2 t'$, and is of the form of a conductive profile on the long mush lengthscale $\boldsymbol{x} = \epsilon \boldsymbol{X}$, modified by a small perturbation on the short lengthscale. Specifically, for $\boldsymbol{X} \sim 1$ we put

$$T = \epsilon T_1 + \epsilon^2 T_2 + \ldots, \tag{4.7}$$

thus on a timescale $t' \sim 1$, T_1 relaxes to the solution of

$$\boldsymbol{u} \cdot \boldsymbol{\nabla} T_1 = \nabla^2 T_1, \tag{4.8a}$$

$$T_1 = 0 \quad \text{on} \quad z = z_l, \quad \frac{\partial T_1}{\partial Z} \to G \quad \text{as} \quad Z \to \infty, \tag{4.8b, c}$$

where G is yet to be found. Note that then $\overline{\partial T_1/\partial n} = G$ on z_l, and in fact this all we strictly require, as actually the compositional field in the mush will be similarly perturbed by a field ϵc_1.

In order to match to the far-field solution, put $\boldsymbol{x} = \epsilon \boldsymbol{X}$, $t = \epsilon^2 t'$, thus

$$T_t + \frac{1}{\epsilon} \boldsymbol{u} \cdot \boldsymbol{\nabla} T = \nabla^2 T, \tag{4.9}$$

with

$$T \to \Delta_\infty \quad \text{as} \quad z \to \infty, \tag{4.10a}$$

$$T = 0, \quad T_z = G \quad \text{on} \quad z = 0 \quad \text{(from matching)}, \tag{4.10b, c}$$

and where $\boldsymbol{\nabla} \equiv \partial/\partial \boldsymbol{x}$. Now the velocity $\boldsymbol{u} \to (0, w(x/\epsilon) + v(x))$ exponentially as $z/\epsilon \to \infty$, where $v(x)$ is the (small) fluid velocity (from the mush) at z_l, i.e. $v = \boldsymbol{u}|_{z_l^-} \cdot \boldsymbol{k}$. By studying (4.9) using multiple scales, we show in Appendix B that T is described, to leading order, by the enhanced transport equation

$$T_t + v T_z = T_{xx} + (1 + G\nu) T_{zz}, \tag{4.11}$$

where ν depends on the scale of the convective fingers. To summarize, we find that the effect of convection in the liquid can be parameterized by the enhanced vertical dispersion coefficient νG in (4.11), where, from Appendices A and B, $G = \partial T/\partial z|_{z_l}$ and $\nu = h^4/315$, h being the (scaled) finger width, $h = O(1)$. Thus, typically, $\nu G \ll 1$, and we will in fact henceforth neglect this term.

4.2. *Basic similarity solution, no convection in the mush*

In the absence of convection, our approximate model is given by (with $z_s = 0$ and $\nu = 0$)

$$s c_t = c_{zz} \quad \text{in} \quad 0 < z < z_l, \tag{4.12a}$$

$$c = 1 \quad \text{on} \quad z = 0, \quad c = 0 \quad \text{on} \quad z = z_l, \tag{4.12b, c}$$

where $s = 1 + S$;

$$T_t = T_{zz} \quad \text{in} \quad z > z_l, \tag{4.13a}$$

$$T \to \Delta_\infty \quad \text{as} \quad z \to \infty, \quad T = 0 \quad \text{on} \quad z = z_l, \quad \frac{\partial T}{\partial z} = -\frac{\partial c}{\partial z} \quad \text{on} \quad z = z_l. \tag{4.13b–d}$$

In terms of similarity variables

$$\eta = \frac{\zeta}{2t^{\frac{1}{2}}}, \tag{4.14}$$

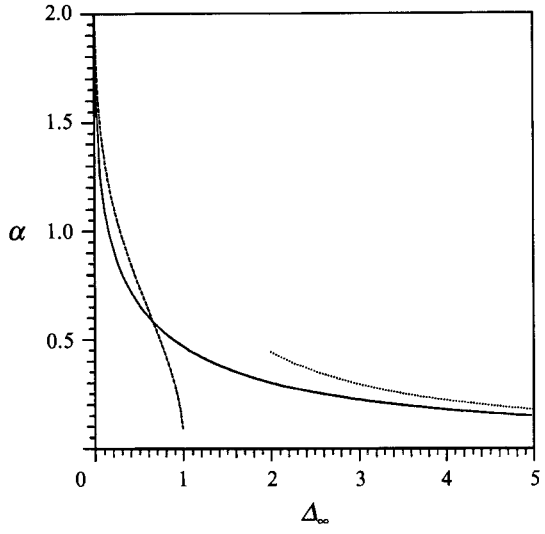

FIGURE 3. The variation of α with Δ_∞ given by (4.16) for $s = 1.25$ (solid curve). The asymptotic relations for small and large Δ_∞ are shown by the dashed and dotted curves respectively.

the solutions are

$$T = \Delta_\infty \left[1 - \frac{\operatorname{erfc}\eta}{\operatorname{erfc}\alpha}\right], \quad \eta \geqslant \alpha, \tag{4.15a}$$

$$c = 1 - \frac{\operatorname{erf} s^{\frac{1}{2}}\eta}{\operatorname{erf} s^{\frac{1}{2}}\alpha}, \quad \eta \leqslant \alpha, \tag{4.15b}$$

and the free boundary location $\alpha = z_l/2t^{\frac{1}{2}}$ is determined by

$$\frac{\Delta_\infty \mathrm{e}^{-\alpha^2}}{\operatorname{erfc}\alpha} = \frac{s^{\frac{1}{2}}\mathrm{e}^{-s\alpha^2}}{\operatorname{erf} s^{\frac{1}{2}}\alpha}. \tag{4.16}$$

Thus α depends on Δ_∞ and s. Selecting values of L, c_p, Γ given in (3.1) and $c_\infty \approx c_E = 0.8$, approximate to NH_4Cl, then $s = 1.25$. In figure 3 we plot $\alpha = \alpha(\Delta_\infty)$ for this value of s. In addition, the asymptotic relations obtained from (4.16) are shown. These are given by

$$\alpha \sim \frac{\pi^{\frac{1}{2}}}{2\Delta_\infty} \quad \text{for} \quad \Delta_\infty \gg 1, \tag{4.17}$$

$$\alpha \sim \left(\frac{1}{s}\log\frac{1}{\Delta_\infty}\right)^{\frac{1}{2}} \quad \text{for} \quad \Delta_\infty \ll 1. \tag{4.18}$$

Worster (1986) has found a similarity solution for the equations with no convective flow in *both* the mush and the liquid regions. Since we have shown that the effect of convection in the liquid can be ignored, our solution is therefore an approximation to Worster's: hence it seems appropriate to compare the two solutions. If we denote Worster's variables with a superscript W then a suitable plot for comparison is λ^W against T_0^W given in figure 8 of Worster (1986). These variables are related to α and Δ_∞ by

$$\alpha = \frac{\lambda^W}{(Le)^{\frac{1}{2}}}, \quad \Delta_\infty = \frac{T_0^W}{T_\infty^L - T_E}. \tag{4.19a, b}$$

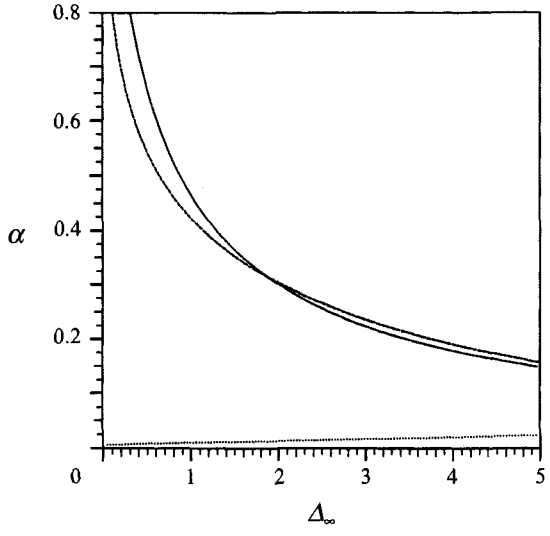

FIGURE 4. A comparison with the similarity solution given by Worster (1986). The dashed curve and the dotted curve are the mush/liquid and solid/mush interface positions derived by Worster. The solid curve shows our results.

For an accurate comparison it is necessary to solve Worster's equations with physical data appropriate to $NH_4Cl.H_2O$. Consequently, we have used the scales in (3.1), and assumed the constants in the solid and liquid phases are equal. Using (4.19) with $T^L_\infty = 9.5\,^\circ\mathrm{C}$, $T_E = -15\,^\circ\mathrm{C}$, the results are shown in figure 4. The dashed and dotted curves, representing the mush/liquid and solid/mush interface positions respectively, are those derived by Worster. Our results (solid curve) compare favourably with his solution; we have supposed that the solid/mush interface is stationary, corresponding to $\beta = 0$ in (3.18).

Since liquid convection is not initiated until after a finite time has elapsed, a similarity solution (including liquid convection) would only strictly be appropriate for times large compared to this onset time. However, this is irrelevant if ν is ignored, and if ν were *not* ignored, (4.11) only has the similarity solution as a limit as $t \to \infty$, in the sense that $T = f(\eta) + O(1/t^{\frac{1}{2}})$.

5. Linear stability

We now return to the reduced model for convection in the mush. The full problem we have to solve is

$$\nabla \cdot \boldsymbol{u} = 0, \tag{5.1a}$$

$$\boldsymbol{u} = -\nabla p + Rc\boldsymbol{k}, \tag{5.1b}$$

$$s\frac{\mathrm{d}c}{\mathrm{d}t} = \nabla^2 c \quad \text{for} \quad z < z_l, \tag{5.1c}$$

with

$$p = c = 0 \quad \text{at} \quad z = z_l, \tag{5.2a}$$

$$u_n = 0, \quad c = 1 \quad \text{at} \quad z = 0, \tag{5.2b, c}$$

and

$$T_t + vT_z = \nabla^2 T \quad \text{for} \quad z > z_l, \tag{5.3}$$

with

$$v = \boldsymbol{u} \cdot \boldsymbol{k}, \quad T = 0 \quad \text{at} \quad z = z_l, \tag{5.4a, b}$$

$$T \to \Delta_\infty \quad \text{as} \quad z \to \infty; \tag{5.4c}$$

and z_l is determined by

$$\left.\frac{\partial T}{\partial n}\right|_{z_l+} = -\left.\frac{\partial c}{\partial n}\right|_{z_l-}. \tag{5.5}$$

The basic similarity solution is given in §4.

Our aim is to find a critical value of R for the onset of convection. However, we need to decide what we mean by stability, since the basic state is time dependent. In this paper we limit ourselves to the concept of quasi-static stability, which is to say that we consider perturbations to the basic state thought of as 'frozen'. In this case time appears as a parameter only, and ordinary linear stability theory can be applied. This has its drawbacks, since the amplitude of convection in a time-evolving system depends on the level of initial perturbation. Thus, while one can reasonably identify a time when small perturbations grow, their manifestation in experiment depends on initial conditions. As a consequence, we do not expect experimental repeatability. Further discussion appears in Emms (1993).

Introducing the stream function ψ via $\boldsymbol{u} = (-\psi_z, \psi_x)$, we have for $0 < z < z_l$

$$\nabla^2\psi = Rc_x, \quad s\frac{\mathrm{d}c}{\mathrm{d}t} = \nabla^2 c, \tag{5.6a, b}$$

and

$$\psi = 0, \quad c = 1 \quad \text{on} \quad z = 0, \tag{5.7a, b}$$

$$\frac{\partial\psi}{\partial n} = 0, \quad c = 0 \quad \text{on} \quad z = z_l. \tag{5.7c, d}$$

For $z_l < z < \infty$

$$T_t + vT_z = \nabla^2 T, \tag{5.8}$$

subject to

$$v = \psi_x, \quad T = 0 \quad \text{on} \quad z = z_l, \tag{5.9a, b}$$

$$T \to \Delta_\infty \quad \text{as} \quad z \to \infty. \tag{5.9c}$$

The basic similarity solution is given by (4.15), that is

$$T = T_0 = \Delta_\infty\left[1 - \frac{\operatorname{erfc}(z/2t^{\frac{1}{2}})}{\operatorname{erfc}\alpha}\right], \tag{5.10a}$$

$$c = c_0 = 1 - \frac{\operatorname{erf}(s^{\frac{1}{2}}z/2t^{\frac{1}{2}})}{\operatorname{erf} s^{\frac{1}{2}}\alpha}, \tag{5.10b}$$

where α is given by (4.16), and $z_l = 2\alpha t^{\frac{1}{2}}$. In the quasi-static stability analysis, we transform to time-varying coordinates

$$x^* = \frac{x}{z_l}, \quad z^* = \frac{z}{z_l}, \quad t^* = \frac{t}{z_l^2}, \tag{5.11a–c}$$

but consider z_l to be fixed.

The linearized equations governing the onset of convection are then (dropping the asterisks) as $z \to \infty$

$$T \to 0; \tag{5.12}$$

for $1 < z < \infty$

$$T_t + \psi_x|_{z=1}\, T_{0z} = \nabla^2 T; \tag{5.13}$$

on $z = 1$

$$\psi_z = 0, \quad T + \zeta T_{0z} = c + \zeta c_{0z} = 0, \tag{5.14a, b}$$

$$T_z + \zeta T_{0zz} = -(c_z + \zeta c_{0zz}); \tag{5.14c}$$

for $0 < z < 1$ $$\nabla^2\psi = R_m c_x, \quad s[c_t + \psi_x c_{0z}] = \nabla^2 c; \tag{5.15a, b}$$

where $$c_0 = 1 - \frac{\operatorname{erf}(s^{\frac{1}{2}}\alpha z)}{\operatorname{erf} s^{\frac{1}{2}}\alpha}, \quad T_0 = \Delta_\infty\left[1 - \frac{\operatorname{erfc}(\alpha z)}{\operatorname{erfc}\alpha}\right], \tag{5.16a, b}$$

and $R_m = z_l R$. Notice that R_m is the ordinary mush Rayleigh number with the mush thickness taken as d. Here $\zeta = \zeta(x, t)$ is the perturbation to the liquid/mush interface.

At the onset of convection, we assume $c_t = 0$ (exchange of stability), and therefore the quasi-static criterion for the onset of convection is that

$$R_m > R_c, \tag{5.17}$$

where R_c is the minimum value of R_m at which the eigenvalue problem

$$\nabla^2 T = -\psi_x|_{z=1}\, T_{0z} \quad \text{for} \quad z > 1, \tag{5.18a}$$

$$\left.\begin{aligned} \nabla^2\psi &= R_m c_x \\ s\psi_x c_{0z} &= \nabla^2 c \end{aligned}\right\} \quad \text{for} \quad 0 < z < 1, \tag{5.18b}$$

$$T \to \Delta_\infty \quad \text{as} \quad z \to \infty, \tag{5.18c}$$

$$\left.\begin{aligned} v_z = 0, \quad T + \zeta T_{0z} &= c + \zeta c_{0z} = 0 \\ T_z + \zeta T_{0zz} &= -(c_z + \zeta c_{0zz}) \end{aligned}\right\} \quad \text{on} \quad z = 1, \tag{5.18d, e, f}$$

$$\psi = c = 0 \quad \text{on} \quad z = 0 \tag{5.18g}$$

has a non-trivial solution.

To solve this numerically, we write ψ, c and T in terms of normal modes e^{ikx}. The liquid equation (5.18a) can be directly integrated to give

$$T = A\, e^{-kz} + \frac{\psi(1)\,\Delta_\infty\, e^{k^2/4\alpha^2 - kz}}{2k \operatorname{erfc}\alpha}\left(\operatorname{erf}\alpha(z - k/2a^2) + e^{2kz}\operatorname{erfc}\alpha(z + k/2\alpha^2)\right), \tag{5.19}$$

where A is an arbitrary constant which determines the size of the eigenfunction. Thus, the following problem remains to be solved:

$$(D^2 - k^2)\psi = R_m k^2 c, \quad (D^2 - k^2)c = -s\psi c_{0z}, \tag{5.20a, b}$$

with boundary conditions

$$c = -T, \quad D\psi = 0 \quad \text{at} \quad z = 1,$$
$$c = 0, \quad \psi = 0 \quad \text{at} \quad z = 0,$$

where $D \equiv d/dz$. The final boundary condition to be satisfied is written as a residual

$$r_b = Dc + DT + 2\alpha^2(s - 1)c = 0 \quad \text{at} \quad z = 1. \tag{5.21}$$

The numerical procedure is then to integrate (5.20) for varying R_m until $r_b = 0$. This gives $R_m = R_m(k, \Delta_\infty, s)$ so that the critical Rayleigh number $R_c = \min_k R_m$.

It we denote the dimensional mush thickness as l_m, the critical mush Rayleigh number criterion is

$$R_m > R_c(\Delta_\infty, s), \tag{5.22}$$

where $$R_m = \frac{\Delta\rho g\, \Pi_0\, l_m}{\mu\kappa_l}. \tag{5.23}$$

For fixed s corresponding to $c_\infty = c_E$ for NH_4Cl, R_c and k_c (the critical wave-number) are functions of Δ_∞. The numerical results are shown in figures 5 and 6.

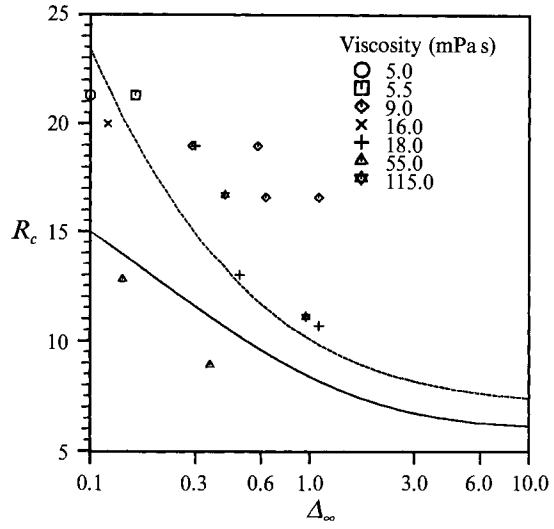

FIGURE 5. The critical Rayleigh number with varying superheat (solid curve). Worster's (1992) theoretical result is shown by the dashed curve. In addition, experimental data (from Tait & Jaupart 1992) for the onset of mush convection are displayed.

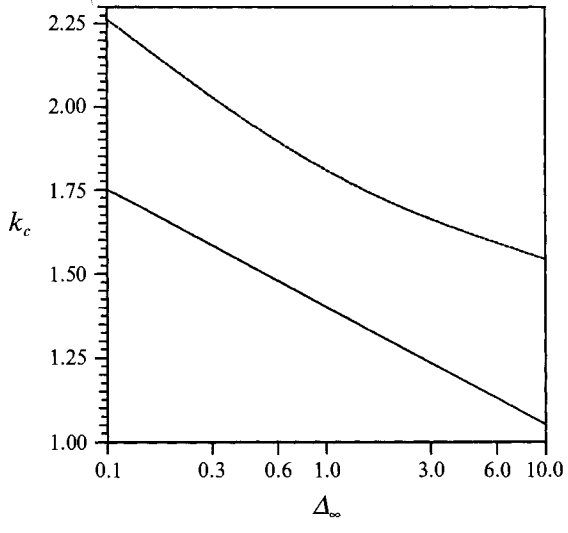

FIGURE 6. The critical wavenumber with varying superheat (solid curve). Worster's (1992) results are shown by the dashed curve.

We calculate the value of the compositional flux G from the similarity solution (4.15) as

$$G = -\frac{\partial c}{\partial z}\bigg|_{z_l^-} = \frac{s^{\frac{1}{2}} e^{-s\alpha^2}}{(\pi t)^{\frac{1}{2}} \operatorname{erf} s^{\frac{1}{2}}\alpha}. \tag{5.24}$$

(Note that the neglect of the enhanced diffusion in (4.11) requires $\nu G \ll 1$.) Therefore $G = G(\alpha, t)$, and an appropriate time to evaluate this function is at the critical time t_c for the onset of convection, given by

$$t_c = \frac{(R_c(\alpha))^2}{4\alpha^2 R^2}. \tag{5.25}$$

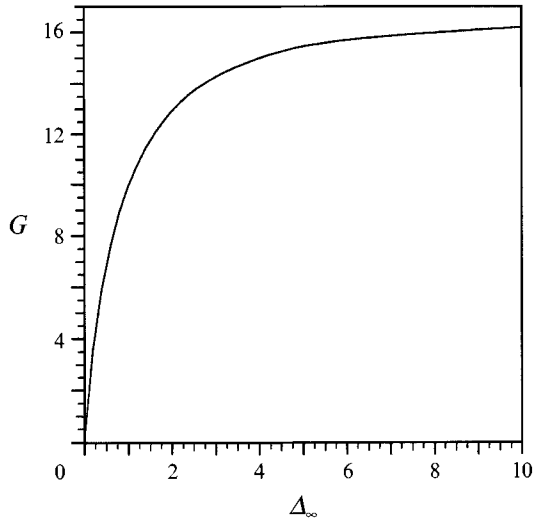

FIGURE 7. The variation of the compositional flux G with Δ_∞ at the onset of convection.

Using (4.16) to find $\alpha = \alpha(\Delta_\infty)$, we plot $G = G(\Delta_\infty)$ in figure 7. As $\Delta_\infty \to \infty$, $G \to 16.5$ since $\alpha \to 0$ and $R_c \to 6.03$ (see below).

Worster (1992) has determined a critical Rayleigh number for the onset of what he calls the 'mushy-layer mode' of instability. This corresponds to the initiation of convection in the mush from stagnant mush and liquid regions. We determine instability from a similarity solution which allows for the finger-like structure in the liquid region, whereas Worster perturbs about a basic *steady* state. however, it is interesting to compare our results.

In figures 5 and 6 a comparison is made between our results and Worster's results shown in figure 11 and 12 of his paper. It can be seen that R_c, k_c compare favourably with his critical Rayleigh number and wavenumber. The critical Rayleigh number R_c in figure 5 tends to a constant as $\Delta_\infty \to \infty$ since to leading order the residual r, given by (5.21), is independent of Δ_∞. This constant was evaluated numerically to be ~ 6.03. In their paper, Tait & Jaupart cite a value of 25 for the critical Rayleigh number in the mush for low superheat. However, their criterion for the onset of convection was the observation of porosity fluctuations in the mush. Thus we would expect a lower theoretical result. There is little variation of the wavenumber k_c with Δ_∞ shown in figure 6 (cf. Worster 1992, figure 11*a*), and it is typically $O(1)$. Thus the cells have a width on the order of the mushy layer thickness. This seems to concur with the observations by Tait & Jaupart of the chimney spacing in the mush. In figure 5 we have also plotted data from the experiments of Tait & Jaupart for the initiation of convection in the mush. It can be seen there is reasonable quantitative agreement with the theoretical results within the scatter of the data.

6. Conclusions

A much simplified model for alloy solidification has been presented, which is appropriate for the study of the onset of convection in the mushy region. By an elaborate scaling procedure we were able to parameterize the convection in the liquid region, and reduce the model still further. The net effect of these simplifications was that the model reduced to the porous-medium convection equations in the mush, and

a diffusion equation for temperature in the liquid. The linear stability of the equations was then analysed, and a Rayleigh-number criterion for the onset of convection in the mush was derived. The results obtained show reasonable quantitative agreement with previous theoretical and experimental work (Worster 1986, 1992; Tait & Jaupart 1992).

Experimental evidence (Chen & Chen 1991; Tait & Jaupart 1992) seems to support the idea that convection is usually initiated from a basic state in which the fluid in the liquid region has a rapidly convecting 'finger-like structure'. As a consequence, we have derived a similarity solution taking this structure into account, and used the solution as the basic time-dependent state. The similarity solution is similar to that given by Worster (1986) for initially quiescent mush and liquid regions.

Once convection has been initiated in the mush we hypothesize that there is a further Rayleigh-number criterion for the onset of channel formation, which leads ultimately to the formation of freckles in the final solidified casting. The determination of this critical Rayleigh number is an area for future work, but it is hoped that the present work provides a foundation on which to build. Current research is aimed at solving the moving boundary problem (5.1)–(5.5) numerically, and comparing with the results presented herein. Examining the evolution of the mass fraction from this solution provides a means to calculate a criterion for the onset of channelling. Specifically, freckles are initiated at z_l if $\phi_t < 0$ there (from (3.6)), i.e. $\mathrm{d}c/\mathrm{d}t < 0$, or equivalently, $w > \dot{z}_l$; that is, freckles are initiated when the fluid flow velocity exceeds that of the freezing isotherm, a condition well known to metallurgists (Flemings 1974).

P.E. acknowledges an SERC earmarked studentship. We thank Grae Worster for providing the data in figures 4–6.

Appendix A. Boundary-layer theory for the liquid region

It will be convenient to introduce the stream function and vorticity defined by $\boldsymbol{u} = (-\psi_z, \psi_x), \omega = -\nabla^2\psi$ respectively, for the rescaled governing equations of the liquid region given by (3.9), (3.10) and (3.12). They can be written (scaling T with ϵ)

$$\nabla^2\omega = \frac{1}{\delta^2}\left[c_x + \frac{R_\alpha}{R_\beta\delta}T_x\right], \tag{A 1a}$$

$$\boldsymbol{u}\cdot\nabla T = \nabla^2 T, \quad \boldsymbol{u}\cdot\nabla c = \frac{1}{Le}\nabla^2 c. \tag{A 1b, c}$$

In (A 1) we have supposed that the liquid 'sees' an effectively stationary liquid/mush interface. Hence we can redefine z so that $z = 0$ is now the position of this interface. To apply the boundary-layer theory of Roberts (1979) we suppose that solute-rich plumes emerge from the mush at regular intervals of $2h$ where $h \sim O(1)$. Appropriate boundary conditions for (A 1) are then

at $x = 0, h$ $$\psi = \psi_{xx} = c_x = T_x = 0, \tag{A 2a}$$

at $z = 0$ $$\psi = \psi_z = T = 0, \tag{A 2b}$$

$$T_z = -\delta c_z = G, \tag{A 2c}$$

as $z \to \infty$ $$c \to 0, \quad T \to \Delta_\infty/\epsilon, \quad \psi_z, \psi_{zz} \to 0. \tag{A 2d}$$

We can assume that G is prescribed in (A 2).

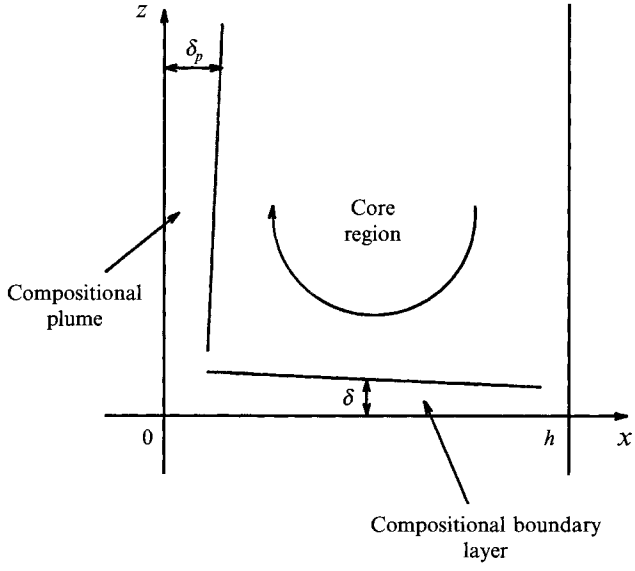

FIGURE 8. The boundary layers in the convective cell.

The boundary-layer theory we construct for the finger-like convection above the mush has a number of differences to previous models for salt fingers (Stern 1975; Schmitt 1979; Howard & Veronis 1987). These models attempt to describe the finger zone that forms between a layer of warm salty water above a layer of cool fresh water. Stern's model assumes an array of fingers of infinite length, with the dependent variables sinusoidal in the horizontal coordinate, and independent of the vertical coordinate. This is probably an accurate description only in the middle of the finger zone. Schmitt (1979) considered time-dependent solutions of Stern's idealized model. He constructed a finite-depth model from fingers with the maximum growth rate, and found good agreement with experimental flux ratios. A different approach was adopted by Howard & Veronis (1987) who constructed a model specifically for fingers of finite depth. The horizontal scale of the fingers was taken to be the buoyancy-layer scale (Veronis 1987). The width of a finger was given by that which gave the maximum buoyancy flux. Each finger was supposed to have the salt concentration of the lower reservoir for an ascending finger, and of the upper reservoir for a descending finger. Eltayeb & Loper (1991) considered the different problem of a single rising salt finger in an attempt to describe the convective plumes that rise out of fully developed chimneys. Again, the horizontal scale of the plume was taken as the buoyancy-layer scale, the actual width of the plume being determined by the maximum buoyancy flux. The concentration in the plume was taken as a constant.

A.1. *Determination of scales*

In what follows, we anticipate that thermal buoyancy is 'small', in a sense to be determined. We shall suppose that the convective cell has the following structure: at $z = 0$ there is a compositional boundary layer of thickness δ, at $x = 0$ there is a rising compositional plume of thickness δ_p, and $x = h$ is a line of symmetry. The anticipated cell structure is shown in figure 8. In the compositional boundary layer convection thus balances diffusion. In the compositional plume a balance of convection with diffusion gives

$$\delta_p^2 = \delta^3. \tag{A 3}$$

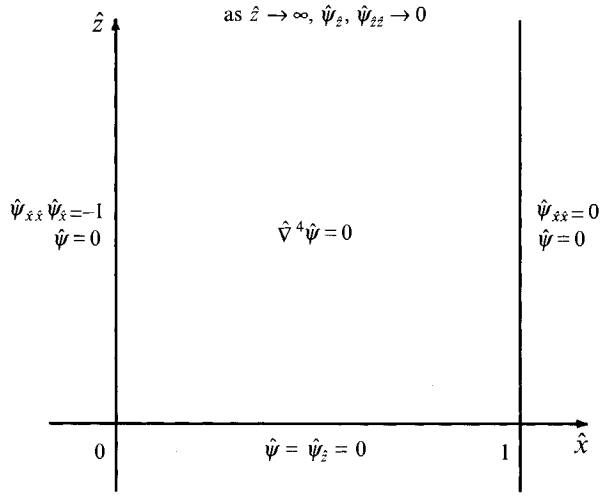

FIGURE 9. The canonical core flow problem.

Additionally a balance of vorticity diffusion with compositional buoyancy in (A 1) yields

$$1/\delta_p = [c]/\delta^2, \tag{A 4}$$

where $[c]$ is the compositional scale in the plume, and we have assumed $\omega \sim O(1)$. Finally we suppose $\int c\mathrm{d}\psi$ is advected around the corner $x = z = 0$, from which we again obtain (A 4), since $\psi \sim \delta^2$ and $c \sim 1$ in the basal boundary layer and $\psi \sim \delta_p$ in the plume. We thus obtain the following scales:

$$[c] \sim \delta^{\frac{1}{2}}, \quad \delta_p \sim \delta^{\frac{3}{2}}. \tag{A 5}$$

In terms of δ (A 1) now become

$$\delta^2\nabla^2\omega = c_x + \frac{R_\rho}{\delta}T_x, \tag{A 6a}$$

$$\boldsymbol{u}\cdot\boldsymbol{\nabla}T = \nabla^2 T, \quad \boldsymbol{u}\cdot\boldsymbol{\nabla}c = \delta^3\nabla^2 c, \tag{A 6b, c}$$

where we have introduced the buoyancy ratio $R_\rho = R_\alpha/R_\beta = \alpha_l\Gamma/\beta_l$. In what follows we assume R_ρ is sufficiently small that thermal buoyancy can be neglected. This requires formally that $R_\rho \ll 1/Le$.

A.2. *The core region*

Regular perturbation expansions in δ for ω, T, c yield $c \sim 0$ to all orders in the core. At leading order

$$\nabla^4\psi = 0, \tag{A 7}$$

providing R_ρ is small enough. The boundary conditions are as in (A 2) except that, at $x = 0$, ψ_{xx} is replaced by $\psi_x\psi_{xx} = -C$ in order to match to the plume (see §A 3). We have solved this problem numerically using a modification of Roberts' (1979) scheme. Here we first rescale

$$\psi = (Ch^3)^{\frac{1}{2}}\hat{\psi}, \quad \boldsymbol{x} = h\hat{\boldsymbol{x}}, \tag{A 8}$$

so that the canonical problem is that shown in figure 9.

We approximate the infinite domain by taking an upper boundary $\hat{z} = 5$. The

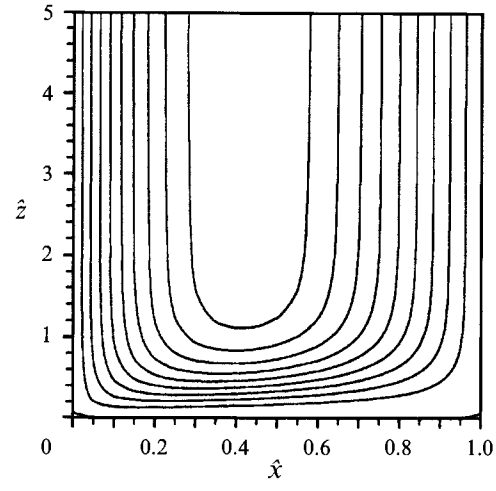

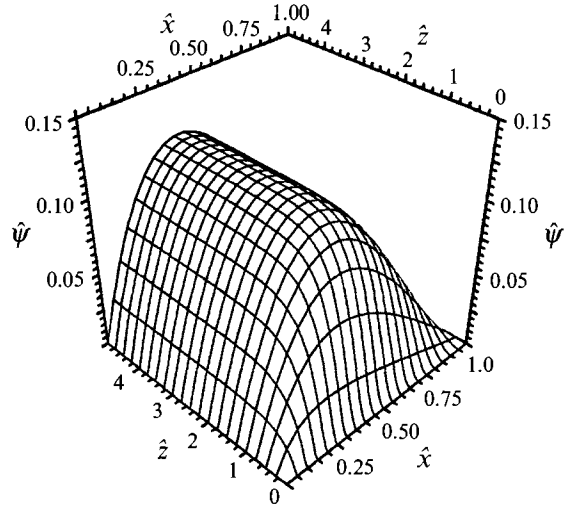

FIGURE 10. The stream function $\hat{\psi}$ in the core region.

streamlines and vorticity in the cell are shown in figures 10 and 11 with a 20×100 mesh. The calculated values of the stream function and vorticity compare well with the asymptotic relations as $\hat{z} \to \infty$. These are given by

$$\hat{\psi} \sim \frac{\hat{x}}{\sqrt{12}}(\hat{x}-1)(\hat{x}-2), \quad \hat{\omega} \sim \sqrt{3}(1-\hat{x}). \tag{A 9}$$

The velocity in the core can then be written in terms of the numerical solution by $\boldsymbol{u} = (Ch)^{\frac{1}{2}}\boldsymbol{u}(x/h, z/h)$.

A.3. *The compositional plume on* $x = 0$

The scales in the plume have been determined as

$$\psi = \delta^{\frac{3}{2}}\Psi, \quad \omega \sim 1, \quad c = \delta^{\frac{1}{2}}\Phi, \quad x = \delta^{\frac{3}{2}}X, \tag{A 10}$$

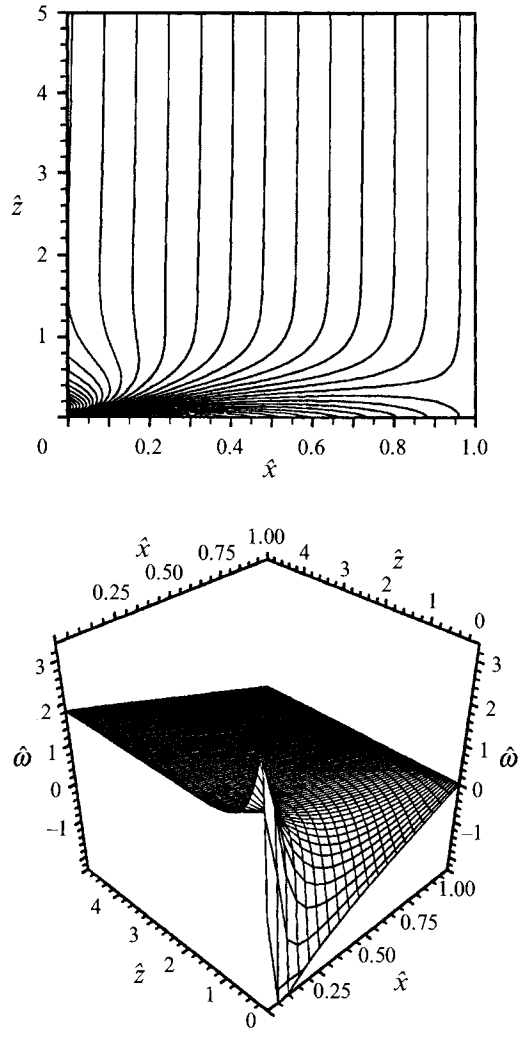

FIGURE 11. The vorticity $\hat{\omega}$ in the core region.

where capital letters denote boundary-layer variables. Substituting into (A 6) we have to leading order

$$\omega_{XX} = \Phi_X, \quad \Psi_X \Phi_z - \Psi_z \Phi_X = \Phi_{XX}, \quad \Psi_{XX} = 0, \tag{A 11a–c}$$

with boundary conditions

at $X = 0$ $\qquad \Psi = \Psi_{XX} = \Phi_X = 0,$

as $X \to \infty$

$$\left.\begin{aligned} \Psi_X &\to v_p(z) \\ \omega &\to \gamma(z) \end{aligned}\right\} \text{ from the core,} \qquad \Phi \to 0 \quad \text{to match to core,} \tag{A 12}$$

and an initial condition at $z = 0$.

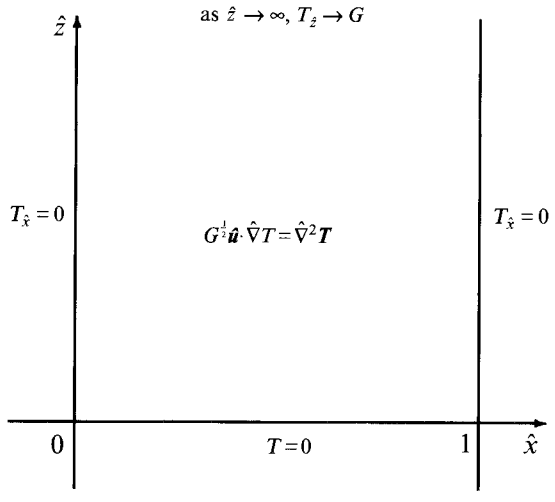

FIGURE 12. The core temperature problem.

Integrating (A 11 *a*, *c*) yields

$$\omega = \gamma(z) - \int_X^\infty \Phi \, \mathrm{d}X \quad \text{where} \quad \int_0^\infty \Phi \, \mathrm{d}X = \gamma(z), \tag{A 13a}$$

$$\Psi = v_p(z)\, X, \tag{A 13b}$$

and in Von Mises coordinates (A 11 *b*) becomes

$$\Phi_\xi = \Phi_{\psi\psi}, \quad \text{where} \quad \xi = \int_0^z v_p(z') \, \mathrm{d}z'. \tag{A 14}$$

From this last relation we see that $C = \int_0^\infty \Phi \, \mathrm{d}\Psi$ is a positive constant. Moreover matching to the core we require $\lim_{x \to 0} \psi_x = v_p(z)$ and $\lim_{x \to 0} \psi_{xx} = -\gamma(z)$. Therefore $-C = -v_p(z)\,\gamma(z) = \psi_x \psi_{xx}$ is the modified boundary condition on $x = 0$.

A.4. *The compositional boundary layer on* $z = 0$

The scales in the compositional layer are

$$\psi = \delta^2 \Psi, \quad \omega \sim 1, \quad c \sim 1, \quad z = \delta Z. \tag{A 15}$$

Substituting into (A 6) we find to leading order

$$\omega_{ZZ} = c_x, \quad \Psi_x c_Z - \Psi_Z c_x = c_{ZZ}, \quad \omega = -\Psi_{ZZ}, \tag{A 16a–c}$$

with boundary conditions

at $Z = 0$ $$\Psi = \Psi_Z = 0, \quad -\overline{\partial c / \partial Z} = G, \tag{A 17a}$$

as $Z \to \infty$ $$\omega \to \omega_c(x) \quad \text{from core solution}, \tag{A 17b}$$

$$c \to 0 \quad \text{to match to core}. \tag{A 17c}$$

The reason for only requiring the average of c_Z to be prescribed is explained further in Appendix B. In Von Mises' coordinates x, Ψ (A 16 *b*) becomes

$$\frac{\partial c}{\partial x} = -\frac{\partial}{\partial \Psi}\left(\Psi_Z \frac{\partial c}{\partial \Psi}\right), \tag{A 18}$$

and the problem is completed by an initial condition at $x = h$.

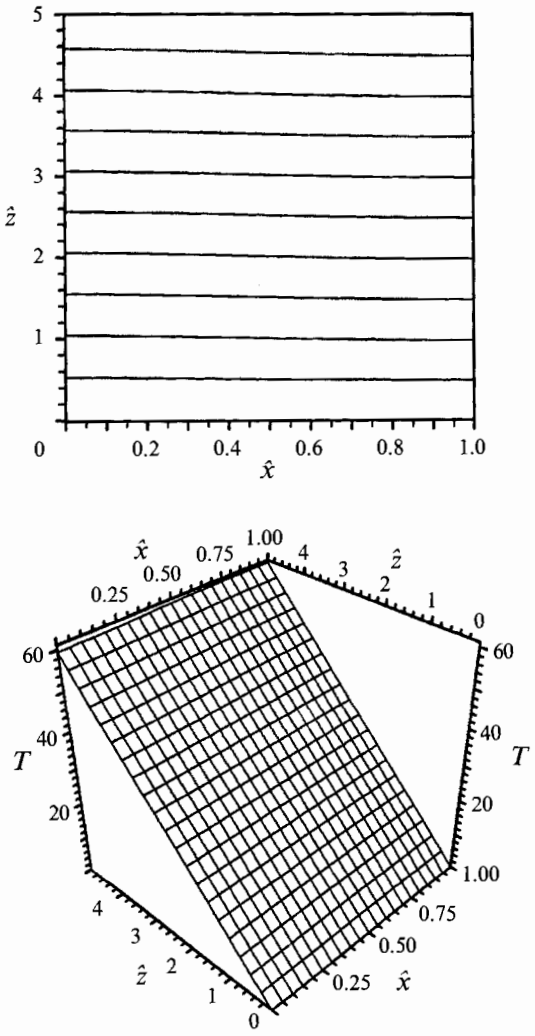

FIGURE 13. The numerical solution to the core temperature problem with $G = 12.0$, corresponding to the compositional flux at the critical Rayleigh number, when $\Delta_\infty = 1.6$.

A.5. *The temperature distribution in the core*

In fact there is no need for us to calculate the boundary-layer solutions since in the compositional layer (A 18) gives

$$\frac{\mathrm{d}}{\mathrm{d}x}\int_0^\infty c\,\mathrm{d}\Psi = \left.\frac{\partial c}{\partial Z}\right|_{z=0}, \tag{A 19}$$

from which it follows that

$$G = -\overline{\frac{\partial c}{\partial Z}} = -\frac{1}{h}\int_0^h \frac{\partial c}{\partial Z}\mathrm{d}x = \frac{C}{h}, \tag{A 20}$$

assuming that $\int c\,\mathrm{d}\Psi$ is advected around the corners. Therefore the numerical solutions in the core gives

$$\boldsymbol{u} = G^{\frac{1}{3}}h\hat{\boldsymbol{u}}(x/h, z/h). \tag{A 21}$$

The vertical lengthscale has been scaled with ϵ, so the appropriate boundary condition at infinity is given by the flux condition on $z = 0$. The core temperature problem is then as displayed in figure 12, and is discussed further in Appendix B. This problem has been solved numerically using the results calculated in figure 10, and a value of $G = 12.0$ corresponding to the onset of convection in the mush at $\Delta_\infty = 1.6$ (figure 7). The solution is displayed in figure 13. To a good approximation, T is just linear, i.e. $T = Gz$.

Appendix B. Homogenization of the temperature in the liquid

Written in terms of the length- and timescales in the *mush*, the liquid temperature equation is

$$T_t + \frac{1}{\epsilon} u(x/\epsilon) \cdot \nabla T = \nabla^2 T, \tag{B 1}$$

where $u \sim O(1)$ is the rescaled velocity field in the liquid, calculated in Appendix A. The boundary conditions are that

$$T = 0 \quad \text{on} \quad z = z_l, \tag{B 2a}$$

$$T \to \Delta_\infty \quad \text{as} \quad z \to \infty. \tag{B 2b}$$

In addition we have $\partial T/\partial n|_{z_l^+} = -\partial c/\partial n|_{z_l^-}$, which determines z_l.

The form of (B 1) suggests a multiple space (and time) scale solution. Specifically, putting

$$t = \epsilon^2 t', \quad x = \epsilon X, \quad T = \epsilon\theta \tag{B 3}$$

(corresponding to the liquid scales introduced in §3.2), then

$$\theta_{t'} + u(X) \cdot \nabla_X \theta = \nabla_X^2 \theta, \tag{B 4}$$

i.e. (A 1*b*) of Appendix A. As indicated there, this *inner* solution must match a far-field outer solution in the liquid where the mush scales are relevant. Specifically, if $u \to (0, w(x/\epsilon) + v(x))$ as $z/\epsilon \to \infty$, this far-field problem is

$$T_t + \{(1/\epsilon) w(x/\epsilon) + v(x)\} T_z = \nabla^2 T, \tag{B 5}$$

and matching requires the same boundary conditions as in (B 2).

We now show how this equation can be solved using a multiple-scale approach. Put

$$x = \epsilon X, \quad z = \epsilon Z, \tag{B 6}$$

and assume

$$T = T(x, z, X, Z, t) \sim T_0 + \epsilon T_1 + \epsilon^2 T_2 + \ldots, \tag{B 7}$$

with each T_i being periodic in X. We obtain the successive problems

$$L(T_0) \equiv wT_{0Z} - (T_{0XX} + T_{0ZZ}) = 0, \tag{B 8a}$$

$$L(T_1) = -wT_{0z} + 2(T_{0xX} + T_{0zZ}) - vT_{0Z}, \tag{B 8b}$$

$$L(T_2) = -wT_{1z} + 2(T_{1xX} + T_{1zZ}) - vT_{1Z} + (\nabla^2 T_0 - vT_{0z} - T_{0t}), \tag{B 8c}$$

where $\nabla^2 \equiv \partial^2/\partial x^2 + \partial^2/\partial z^2$. We can take $w(X)$ as periodic of zero mean, specifically suppose

$$w = \sum_1^\infty w_n \cos nX, \tag{B 9}$$

and define V periodic with zero mean by

$$V_{XX} = -w, \quad V = \sum_{1}^{\infty} \frac{w_n}{n^2} \cos nX. \tag{B 10}$$

Then
$$T_0 = T_0(x, z, t) \tag{B 11}$$

solves (B 8a), and
$$T_1 = -T_{0z} V \tag{B 12}$$

solves (B 8b), suppressing secular terms proportional to Z. Thus we find

$$L(T_2) = wVT_{0zz} - 2T_{0xz} V_X + \nabla^2 T_0 - T_{0t} - vT_{0z}. \tag{B 13}$$

In order to obtain a solution periodic in X with zero mean and $\partial T_2/\partial Z \to 0$ at ∞, we require $\overline{L(T_2)} = 0$, where the overbar denotes the horizontal spatial average. With the stream function ψ defined by $w = \psi_X$, thus $V_X = -\psi$, we have

$$\overline{wV} = -\overline{V_{XX} V} = \tfrac{1}{2}\overline{V_X^2} = \tfrac{1}{2}\overline{\psi^2}. \tag{B 14}$$

It follows that in order for the right-hand side of (B 13) to have zero mean in X, $T = T_0$ must satisfy the solvability condition

$$T_t + vT_z = T_{xx} + (1 + \tfrac{1}{2}\overline{\psi^2})\, T_{zz}. \tag{B 15}$$

The enhanced vertical diffusivity is entirely analogous to Taylor dispersion (Taylor 1953). Using (A 8), (A 9) and (A 20) of Appendix A, we find that

$$\tfrac{1}{2}\overline{\psi^2} = G\nu \tag{B 16}$$

where $G = \partial T/\partial z|_{z_l}$ and the geometric factor ν is given by

$$\nu = h^4/315. \tag{B 17}$$

Thus in practice the enhancement is likely to be small.

REFERENCES

AMBERG, G. 1991 Computation of macrosegregation in an iron-carbon cast. *Intl J. Heat Mass Transfer* **34**, 217–227.

AMBERG, G. & HOMSY, G. M. 1993 Nonlinear analysis of buoyant convection in binary solidification with application to channel formation. *J. Fluid Mech.* **252**, 79–98.

BECKERMANN, C. & VISKANTA, R. 1988 Double-diffusive convection during dendritic solidification of a binary mixture. *PhysicoChem. Hydrodyn* **10**, 195–213.

BENNON, W. D. & INCROPERA, F. P. 1987*a* A continuum model for momentum, heat and species transport in binary solid-liquid phase change systems – I. Model formulation. *Intl J. Heat Mass Transfer* **30**, 2161–2170.

BENNON, W. D. & INCROPERA, F. P. 1987*b* The evolution of macrosegregation in statically cast binary ingots. *Metall. Trans.* **18B**, 611–616.

CHEN, C. F. & CHEN, F. 1991 Experimental study of directional solidification of aqueous ammonium chloride solution. *J. Fluid Mech.* **227**, 567–586.

COPLEY, S. M., GIAMEI, A. F., JOHNSON, S. M. & HORNBECKER, M. F. 1970 The origin of freckles in unidirectionally solidified castings. *Metall. Trans* **1**, 2193–2204.

DREW, D. A. & WOOD, R. T. 1985 *Overview and Taxonomy of Models and Methods for Workshop on Two-Phase Flow Fundamentals.* National Bureau of Standards, Gaithersburg, Maryland.

ELTAYEB, L. A. & LOPER, D. E. 1991 On the stability of vertical double-diffusive interfaces. Part 1. A single plane interface. *J. Fluid Mech.* **228**, 149–181.

EMMS, P. W. 1993 Compositional convection and freckle formation in a solidifying binary alloy. D.Phil. thesis, Oxford University.

FLEMINGS, M. C. 1974 *Solidification Processing*. McGraw-Hill.

FLEMINGS, M. C. & NEREO, G. E. 1967 Macrosegregation: Part I. *Trans. Metall. Soc. AIME* **329**, 1449–1461.

FOWLER, A. C. 1985 The formation of freckles in binary alloys. *IMA J. Appl. Maths* **35**, 159–174.

FUJII, T., PROCTOR, D. R. & FLEMINGS, M. C. 1979 Macrosegregation in a multi-component low steel alloy. *Metall. Trans.* **10B**, 331–339.

GANESAN, S. & POIRIER, D. R. 1990 Conservation of mass and momentum for the flow of interdendritic liquid during solidification. *Metall. Trans.* **21B**, 173–181.

HILLS, R. N., LOPER, D. E. & ROBERTS, P. H. 1983 A thermodynamically consistent model of a mushy zone. *Q. J. Mech. Appl. Maths* **36**, 505–539.

HOWARD, L. N. & VERONIS, G. 1987 The salt-finger zone. *J. Fluid Mech.* **183**, 1–23.

HUPPERT, H. E. 1990 The fluid mechanics of solidification. *J. Fluid Mech.* **212**, 209–240.

HUPPERT, H. E. & WORSTER, M. G. 1985 Dynamic solidification of a binary melt. *Nature* **314**, 703–707.

JACOBS, J. A. 1953 The earth's inner core. *Nature* **172**, 297–298.

KOU, S., POIRIER, D. R. & FLEMINGS, M. C. 1978 Macrosegregation in rotated remelted ingots. *Metall. Trans.* **9B**, 711–719.

LOPER, D. E. & ROBERTS, P. H. 1978 On the motion of an iron alloy core containing a slurry I. General theory. *Geophys. Astrophys. Fluid Dyn.* **9**, 289–321.

LOPER, D. E. & ROBERTS, P. H. 1980 On the motion of an iron-alloy core containing a slurry II. A simple model. *Geophys. Astrophys. Fluid Dyn.*, **16**, 83–127.

LOPER, D. E. & ROBERTS, P. H. 1981 Compositional convection and the gravitationally powered dynamo. In *Stellar and Planetary Magnetism* (ed. A. M. Soward), pp. 297–327. Gordon and Breach.

MAPLES, A. L. & POIRIER, D. R. 1984 Convection in the two-phase zone of solidifying alloys. *Metall. Trans.* **15B**, 163–172.

MCDONALD, R. J. & HUNT, J. D. 1969 Fluid motion through the partially solid regions of a casting and its importance in understanding A-type segregation. *Trans. Metall. Soc. AIME* **245**, 1993–1997.

MCDONALD, R. J. & HUNT, J. D. 1970 Convective fluid motion within the interdendritic liquid of a casting. *Metall. Trans* **1**, 1787–1788.

MEHRABIAN, R., KEANE, M. & FLEMINGS, M. C. 1970*a* Experiments on macrosegregation and freckle formation. *Metall. Trans.* **1**, 3238–3241.

MEHRABIAN, R., KEANE, M. & FLEMINGS, M. C. 1970*b* Interdendritic fluid flow and macrosegregation; Influence of gravity. *Metall. Trans.* **1**, 1209–1220.

NEILSON, D. G. & INCROPERA, F. P. 1991 Unidirectional solidification of a binary alloy and the effects of induced fluid motion. *Intl J. Heat Mass Transfer* **34**, 1717–1732.

NI, J. & BECKERMANN, C. 1991 A volume-averaged two-phase model for transport phenomena during solidification. *Metall. Trans.* **22B**, 349–361.

PROCTOR, M. R. E. 1981 Steady subcritical thermohaline convection. *J. Fluid Mech.* **105**, 507–521.

RIDDER, S. D., KOU, S. & MEHRABIAN, R. 1981 Effect of fluid flow on macrosegregation in axisymmetric ingots. *Metall. Trans.* **12B**, 435–447.

ROBERTS, G. O. 1977 Fast viscous convection. *Geophys. Astrophys. Fluid Dyn.* **8**, 197–233.

ROBERTS, G. O. 1979 Fast viscous Bénard convection. *Geophys. Astrophys. Fluid Dyn.* **12**, 235–272.

ROBERTS, P. H. & LOPER, D. E. 1983 Towards a theory of the structure and evolution of a dendrite layer. In *Stellar and Planetary Magnetism* (ed. A. M. Soward), pp. 329–349. Gordon and Breach.

SAMPLE, A. & HELLAWELL, A. 1982 The effect of mold precession on channel and macro-segregation in ammonium chloride-water analog castings. *Metall. Trans.* **13B**, 495–501.

SAMPLE, A. K. & HELLAWELL, A. 1984 The mechanisms of formation and prevention of channel segregation during alloy solidification. *Metall. Trans.* **15A**, 2163–2173.

SARAZIN, J. R. & HELLAWELL, A. 1988 Channel formation in Pb–Sn, Pb–Sb, and Pb–Sn–Sb alloy ingots and comparison with the system NH_4Cl-H_2O. *Metall. Trans.* **19A**, 1861–1871.

SCHMITT, R. W. 1970 Flux measurements on salt fingers at an interface. *J. Mar. Res.* **37**, 419–437.

STERN, M. E. 1975 *Ocean Circulation Physics*. Academic.

SZEKELY, J. & JASSEL, A. S. 1978 Experimental and analytical study of the solidification of a binary dendritic system. *Metall. Trans.* **9B**, 389–398.

TAIT, S. & JAUPART, C. 1992 Compositional convection in a reactive crystalline mush and melt differentiation. *J. Geophys. Res.* **97**(B5), 6735–6756.

TAYLOR, G. I. 1953 Dispersion of soluble matter in solvent flowing slowly through a tube. *Proc. R. Soc. Lond* A **219**, 186–203.

THOMPSON, M. E. & SZEKELY, J. 1988 Mathematical and physical modelling of double-diffusive convection of aqueous solutions crystallizing at a vertical wall. *J. Fluid Mech.* **187**, 409–433.

TURNER, J. S. 1973 *Buoyancy Effects in Fluids*. Cambridge University Press.

VERONIS, G. 1987 The role of the buoyancy layer in determining the structure of salt fingers. *J. Fluid Mech.* **180**, 327–342.

WOODRUFF, D. P. 1973 *The Solid–Liquid Interface*. Cambridge University Press.

WORSTER, M. G. 1986 Solidification of an alloy from a cooled boundary. *J. Fluid Mech.* **167**, 481–501.

WORSTER, M. G. 1991 Natural convection in a mushy layer. *J. Fluid Mech.* **224**, 335–359.

WORSTER, M. G. 1992 Instabilities of the liquid and mushy regions during solidification of alloys. *J. Fluid Mech.* **237**, 649–669.